



RESEARCH PAPER



Structural determinants for subnanomolar inhibition of the secreted aspartic protease Sapp1p from *Candida parapsilosis*

Jiří Dostál^a, Jiří Brynda^a, Lucie Vaňková^b, Syeda Rehana Zia^c, Iva Pichová^a , Olga Heidingsfeld^{a,d} and Martin Lepšík^a 

^aInstitute of Organic Chemistry and Biochemistry, Czech Academy of Sciences, Prague, Czech Republic; ^bLaboratory of Ligand Engineering, Institute of Biotechnology, Czech Academy of Sciences, v.v.i., BIOCEV Research Center, Vestec, Czech Republic; ^cDepartment of Chemistry, University of Karachi, Karachi, Pakistan; ^dDepartment of Biochemistry, Faculty of Science, Charles University in Prague, Prague, Czech Republic

ABSTRACT

Pathogenic *Candida albicans* yeasts frequently cause infections in hospitals. Antifungal drugs lose effectiveness due to other *Candida* species and resistance. New medications are thus required. Secreted aspartic protease of *C. parapsilosis* (Sapp1p) is a promising target. We have thus solved the crystal structures of Sapp1p complexed to four peptidomimetic inhibitors. Three potent inhibitors (K_i : 0.1, 0.4, 6.6 nM) resembled pepstatin A (K_i : 0.3 nM), a general aspartic protease inhibitor, in terms of their interactions with Sapp1p. However, the weaker inhibitor (K_i : 14.6 nM) formed fewer nonpolar contacts with Sapp1p, similarly to the smaller HIV protease inhibitor ritonavir (K_i : 1.9 μ M), which, moreover, formed fewer H-bonds. The analyses have revealed the structural determinants of the subnanomolar inhibition of *C. parapsilosis* aspartic protease. Because of the high similarity between Saps from different *Candida* species, these results can further be used for the design of potent and specific Sap inhibitor-based antimycotic drugs.

ARTICLE HISTORY

Received 19 January 2021
Revised 11 March 2021
Accepted 17 March 2021

KEYWORDS

Inhibitor; peptidomimetics; crystal structure; hydrogen bonds; noncovalent interactions

Introduction

Pathogenic yeasts of the *Candida* species are among the leading causative agents of hospital-acquired yeast infections as they are often spread on the hands of health-care personnel. They prevail in specific hosts and environments such as low-birth-weight infants in neonatal intensive-care units¹. Three classes of antifungal drugs (azoles, polyenes and echinocandins) are recommended for the treatment of candidiasis, mainly caused by *C. albicans*². However, their effectiveness is hampered by the growth of other species, most notably *C. parapsilosis*, as well as the development of resistance due to biofilm formation^{3,4}. It is thus necessary to develop new types of antifungal drugs against new molecular targets.

Secreted aspartic proteases (Saps) of *Candida* species are extracellular enzymes with broad substrate specificity that enable the yeasts to overcome barriers used by the human host to prevent invasive infection⁵. Moreover, Saps enhance the yeast virulence by degrading the host proteins involved in defence. They are also required for proper yeast adhesion during biofilm development⁶. Saps are differentially transcribed depending on ambient conditions or disease progression⁷. Their inhibition, albeit by aspartic protease inhibitors developed against other enzymes, e.g. HIV-1 protease, in combination with administration of other antifungal drugs, has reduced the formation of *C. albicans* biofilms and disrupted their mature form⁴. The effect of these inhibitors in the reduction of oropharyngeal candidiasis and other surface mycoses has been reported in several studies^{8–15}. The structure-based discovery and optimisation of indolone derivatives as Sap2 inhibitors

is promising for the treatment of resistant *Candida albicans* infections^{16,17}. *C. parapsilosis*, as a major non-*albicans* *Candida* pathogen, possesses at least three Sap isoenzymes, of which Sapp1p appears to contribute most significantly to the host-cell damage and the survival of *C. parapsilosis* in the host^{18,19}. Therefore, the development of specific Sap inhibitors is an important pharmaceutical goal.

Understanding the three-dimensional structure of aspartic proteases is a key to successful inhibitor design, as was exemplified in the 1990s for HIV protease in search for anti-AIDS drugs²⁰. Yeast Saps are similar in structure to pepsin-like aspartic proteases²¹. They are arranged as two domains, consisting mostly of β -sheets, with a spacious substrate-binding cleft between them (Figure 1(A)). Each domain contributes one DT(S)G triad to the active site, with the aspartate residue indispensable for catalysis. The central part of the extended active site is covered by an anti-parallel β -sheet, called flap. Peptidic substrates and peptidomimetic inhibitors span the active-site cavity in an extended conformation, placing their amino-acid side chains P4-P1 and P1'-P4' into their respective S4-S1 and S1'-S3' pockets (Figure 1(B)). Sapp1p is an enzyme with wide substrate specificity²² and relatively open substrate-binding cleft²³. The entrance to the substrate-binding site is lined with four entrance loops (N-ent loop 1, N-ent loop 2, C-ent loop 1 and C-ent loop 2; Figure 1(A)), which modulate inhibitor affinities. Two disulphide bridges (Cys 47 – Cys 53 and Cys 258 – Cys 292) contribute to the stability of the structure.

Peptidomimetic aspartic protease inhibitors combine an uncleavable isostere of the peptide bond, bound in the S1/S1'

CONTACT Dr. Martin Lepšík  lepsik@uochb.cas.cz; Dr. Iva Pichová  iva.pichova@uochb.cas.cz  Institute of Organic Chemistry and Biochemistry, Czech Academy of Sciences, Flemingovo náměstí 2, Prague 166 10, Czech Republic

© 2021 The Author(s). Published by Informa UK Limited, trading as Taylor & Francis Group.

This is an Open Access article distributed under the terms of the Creative Commons Attribution-NonCommercial License (<http://creativecommons.org/licenses/by-nc/4.0/>), which permits unrestricted non-commercial use, distribution, and reproduction in any medium, provided the original work is properly cited.

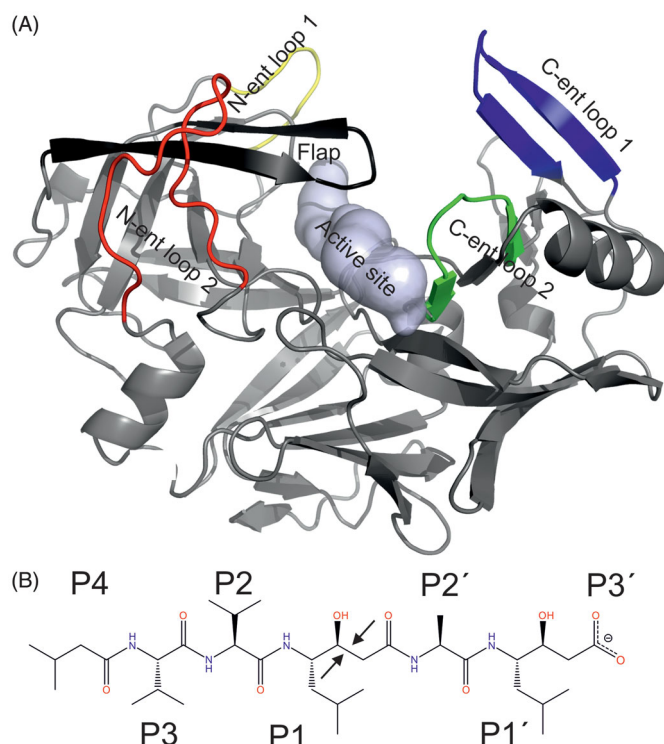


Figure 1. The structure of Sapp1p and pepstatin A. (A) The overall structure of the Sapp1p complex with pepstatin A (PDB: 3FV3)²³, showing the volume of the substrate/inhibitor-binding pocket, with four loops and the flap coloured. (B) The structure of pepstatin A (isovaleric acid-valine-valine-statine-alanine-statine), a general aspartic-protease inhibitor. The arrows mark the position of the peptide-substrate C-N scissile bond, which is replaced in pepstatin A by an uncleavable C-C bond in statine. The residues towards the N-terminus are designated as the non-prime side, whereas those towards the C-terminus are the prime side. In Schechter-Berger nomenclature, the P4-P1, P1'-P3' side chains are positioned into their respective S4-S1, S1'-S3' enzyme subsites. In pepstatin A, the central statine (Sta) moiety contains a non-scissile bond with two additional carbon atoms with respect to a standard amino acid; therefore, the prime-side residues are positioned differently (c.f. Figure 2).

region, with amino-acid mimics in adjacent positions. The most thoroughly studied inhibitor of this type is pepstatin A (Figure 1(B)), a general inhibitor of aspartic proteases. Pepstatin A contains a central statine residue, which acts as a transition-state analogue (Figure 1(B))^{5,24}. Pepstatin A inhibits most of aspartic proteases in subnanomolar concentrations (K_i of 0.3 nM for Sapp1p)²⁵. It has inspired the design and synthesis of numerous inhibitors targeted towards pharmacologically important proteases. Recently, novel types of macrocyclic mimetics designed using the knowledge of pepstatin A conformation in the binding cavity were found to efficiently inhibit human aspartic protease cathepsin D²⁶ which is structurally similar to Saps. A series of pepstatin A based inhibitors varied at the P3, P2 and P2' positions were targeted against Sap1, Sap3, Sap5, and Sap6 from *C. albicans*²⁷. Other phenylstatine (Pst)-containing pepstatin A inspired inhibitors were tested with Sap1 from *C. albicans*, Sapp1p from *C. parapsilosis*, and Sapt1p from *C. tropicalis*²⁵. The K_i values of the Pst-containing inhibitors of this series (designated as KB32, KB70, KB74 and KB75) ranged from 0.1 nM to 14.6 nM for Sapp1p²⁵. As alluded to above, Saps from different pathogenic *Candida spp.* are also inhibited by clinically used HIV-1 protease (PR) inhibitors, but in micromolar concentrations^{8,25,28-30}. The best *in vitro* Sapp1p inhibition was achieved using the nonpeptidic HIV PR inhibitor ritonavir (K_i 1.9 μ M)²⁵. In our previous work, we determined the structures of Sapp1p and the related Sapp2p in complex with pepstatin A^{23,31} and Sapp1p with ritonavir³². These structural

studies shed light into the binding modes but did not quantify the molecular determinants for differential affinity.

This work presents four crystal structures of Sapp1p complexes with four Pst-containing pepstatin-based inhibitors. The protein-ligand hydrogen bonding and nonpolar interactions in these complexes have been analysed in detail and compared with Sapp1p/pepstatin A²³ and Sapp1p/ritonavir³² complexes. This analysis has made it possible to pinpoint the structural determinants responsible for the subnanomolar inhibition of this enzyme.

Materials and methods

Sapp1p purification

Sapp1p, used in this study, was an authentic enzyme purified from *C. parapsilosis* culture supernatant, as described previously^{23,32}. *C. parapsilosis* strain P69 from the mycological collection of the Faculty of Medicine, Palacky University, Olomouc, Czech Republic was cultivated in the YCB-BSA medium consisting of 1.2% (w/v) Yeast Carbon Base (Difco), 0.2% (w/v) BSA and 15 mM sodium citrate, pH 4. The culture supernatant obtained after approximately 70 h of cultivation and the removal of the cells by centrifugation (5000 g, 15 min) was subjected to ion-exchange chromatography, followed by gel filtration. Finally, Sapp1p and Sapp2p proteases were separated using chromatofocusing. Enzyme-activity assays were performed using the fluorogenic substrate Dabcyl-Glu-His-Val-Lys-Leu-Val-Glu-EDANS, which is cleaved at the Leu-Val bond by Sapp1p³³.

Crystallisation and data collection

The complexes of Sapp1p with inhibitors were prepared and crystallised as follows. Purified Sapp1p (15 mg mL⁻¹) was incubated for 30 min at room temperature with a twofold molar excess of the inhibitor (applied as a DMSO solution) in 15 mM sodium citrate, pH 3.75 (the final DMSO concentration did not exceed 2%). The mixture was centrifuged for 5 min at 16,000 g. The initial crystallisation trials were performed with the help of a Gryphon crystallisation workstation (Art Robbins Instruments) by the sitting-drop vapour-diffusion method at 18 °C in 96-well plates; 0.2 μ l of protein solution were mixed with 0.2 μ l of well solution, and the mixture was equilibrated over a 200 μ l reservoir solution. PEGs Suite I and JCSG Core I Suite (QIAGEN) were used for the crystallisation condition screen. The initial microcrystals of Sapp1p with inhibitors appeared in several days. The subsequent optimisation of crystallisation conditions involved a change to the hanging-drop mode, which was performed in NeXtal plates (Qiagen). The ratio of the protein to the precipitant solution was 2:1 for Sapp1p with KB32 and KB74 complexes and 1:1 for Sapp1p with KB70 and KB75 complexes. The final crystals were obtained under the following conditions. For the complexes of Sapp1p with KB32 and KB70, they were: 0.1 M MES pH 6.5, 40% PEG 200; for the complexes of Sapp1p with KB74 and KB75: 0.1 M MES pH 6.5, 30% PEG 400. The crystals were flash-cooled in liquid nitrogen with the precipitant solution as a self-cryoprotectant.

Diffraction data were collected at 100 K on MX 14.1 operated by the Joint Berlin MX-Laboratory at the BESSY II electron-storage ring in Berlin-Adlershof, Germany³⁴.

Diffraction data for Sapp1p_KB74 were processed, integrated, and reduced using XDS and scaled by XSCALE from the XDS suite, whereas the data for the other complexes were integrated by mosflm and scaled by the CCP4 package SCALA³⁵. The crystals belonged to the P2₁2₁2₁ or P6₂22 space group and contained

Table 1. Crystal data and diffraction data collection and refinement statistics

	Sapp1p-KB70	Sapp1p-KB75	Sapp1p-KB32	Sapp1p-KB74
Crystal data				
Space group	<i>P</i> ₆ ₂ ₂	<i>P</i> ₆ ₂ ₂	<i>P</i> ₂ ₁ ₂ ₁	<i>P</i> ₂ ₁ ₂ ₁
a, b, c (Å)	172.62, 172.62, 253.25	172.62, 172.62, 253.25	87.26, 87.29, 157.95	87.25, 87.35, 157.68
α, β, γ (°)	90.00, 90.00, 120.00	90.00, 90.00, 120.00	90.00, 90.00, 90.00	90.00, 90.00, 90.00
Molecules per asymmetric unit	4	4	4	4
Max. resolution (Å)	1.70	1.80	1.30	1.35
Data collection and processing				
Wavelength (Å)	0.9184	0.9184	0.9184	0.9184
Resolution limits (Å)	50.00–1.70 (1.75–1.70)	50.00–1.80 (1.85–1.80)	50.0–1.25 (1.28–1.25)	50.00–1.35 (1.43–1.35)
No. of observed reflections	3494125 (214086)	1961990 (87469)	1554178 (74828)	838724 (115425)
No. of unique reflections	234657 (15854)	202267 (13667)	323787 (18707)	253539 (38187)
Multiplicity	14.5 (13.5)	9.7 (6.4)	4.8 (4.0)	3.3 (3.0)
R _{meas.}	0.098 (1.67)	0.13 (1.10)	0.073 (0.708)	0.064 (0.537)
R _{merge} ^[a]	0.094 (1.61)	0.113 (0.92)	0.060 (0.548)	0.054 (0.443)
CC _{1/2}	100.0 (68.6)	99.7 (52.3)	99.9 (65.3)	99.9 (78.0)
Completeness (%)	98.3 (90.9)	99.3 (78.2)	84.3 (76.5)	96.2 (90.3)
<I/σI>	19.7 (1.85)	12.1 (0.8)	11.4 (1.4)	14.5 (2.35)
Wilson B-factor (Å ²)	31.1	22.9	10.2	17.1
Refinement statistics				
Resolution (Å)	34.58–1.70 (1.74–1.70)	18.45–1.80 (1.85–1.80)	23.14–1.3 (1.34–1.30)	78.84–1.35 (1.39–1.35)
No. of reflections in working set	221558 (14326)	192014 (12888)	274147 (19750)	240826 (14664)
No. of reflections in test set	11694 (759)	10179 (656)	14594 (1050)	12767 (777)
R _{work} ^[b] (%)	17.9 (27.5)	20.2 (31.0)	16.2 (24.7)	16.4 (24.7)
R _{free} (%)	19.7 (28.1)	22.2 (30.6)	18.0 (26.1)	18.6 (24.9)
Average B-factor (Å ²)	34.7	29.0	13.2	11.4
RMSD bond length (Å)	0.013	0.012	0.013	0.012
RMSD angle (°)	2.0	1.9	1.6	1.6
Number of atoms in AU (protein/inhibitor/solvent molecules)	10246/220/985	10198/212/1073	10406/223/1649	10393/160/1101
Ramachandran plot				
Most favoured regions (%)	97.77	97.47	98.37	98.22
Additional allowed regions (%)	2.23	2.53	1.63	1.78
Disallowed regions (%)	0.0	0.0	0.0	0.0
PDB code	7AGB	7AGD	7AGE	7AGC

^[a]R_{merge} = $\frac{\sum_{\text{hkl}} \sum_i |I_i(\text{hkl}) - \langle I(\text{hkl}) \rangle|}{\sum_{\text{hkl}} \sum_i I_i(\text{hkl})}$. ^[b]R_{work} = $\frac{\sum |F_{\text{calc}}| - |F_{\text{obs}}|/\sum |F_{\text{obs}}|}{\sum |F_{\text{obs}}|} \cdot 100$.

four molecules in the asymmetric unit, with a solvent content of approximately 47%. Crystal parameters and data-collection statistics are given in Table 1.

Structure solution

All structures were solved by molecular replacement with CCP4 Molrep³⁵, using available structures of identical proteins (3FV3)²³. The initial models were refined through several cycles of manual building using Coot and automated refinement with CCP4 REFMAC5³⁶. Structural data were visualised in PyMOL. Atomic coordinates and structure factors were deposited in the Protein Data Bank under the codes 7AGB, 7AGC, 7AGD and 7AGE (Table 1).

The analysis of enzyme–inhibitor interactions

Four crystal structures of Sapp1p in complex with inhibitors (KB32, KB70, KB74 and KB75) and Sapp1p/pepstatin A complex (PDB: 3FV3)²³ were analysed for protein–ligand hydrogen bonds and nonpolar interactions using Protein–Ligand Interaction Profiler PLIP³⁷ for non-peptidic parts of the ligands and UCSF CHIMERA³⁸ for peptidic parts of the ligands. Prior to the analyses, the structures were protonated using CHIMERA. For the catalytic Asp dyad, a probable protonation state was assigned based on our previous quantum chemical calculations in Sapp2p/inhibitor complexes³¹ (Figure 2). The cut-off atom–atom distances were set to 4.1 Å; for hydrogen bonding, the minimum D–H···A angle was set to 100°. The analyses were carried out for chains A of the structures.

PyMol version 1.7.6.3 (Molecular Graphics System, Version 2.0 Schrödinger, LLC) was used for visualisation.

Results

The structures and binding modes in Sapp1p-inhibitor complexes

The crystal structures of Sapp1p complexes with four pepstatin-based inhibitors, KB70 (tert-butyl-oxycarbonyl-valine-valine-phenylstatine-alanine-phenylstatine-NH₂), KB32 (tert-butyl-oxycarbonyl-valine-valine-phenylstatine-alanine-phenylstatine-O), KB75 (tert-butyl-oxycarbonyl-valine-valine-phenylstatine-alanine-(3R, 4R)-phenylstatine-OMe) and KB74 (tert-butyl-oxycarbonyl-valine-valine-phenylstatine-alanine-OMe), were obtained at the resolution of 1.25–1.80 Å. Four nearly identical protein–ligand chains were present in the asymmetric unit cell, differing only in the conformations of the C-terminal phenylstatine (Pst) backbone (except for KB74, which contains only the central Pst residue). The overall structures of all the complexes were similar to each other (with the RMSD being 0.191–0.293 Å) and also to the Sapp1p complex with pepstatin A (the PDB entry 3FV3)²³.

The binding modes of all pepstatin-based inhibitors towards Sapp1p were nearly identical on the non-prime side (P4–P1) and in the P2' position. The main differences appeared in the P1' and P3' regions (Figure 2(A)); they were caused by the different moieties and their stereochemistry. Ritonavir utilises a similar backbone binding mode to pepstatin A, including its isosteric hydroxyl and P2, P1 side chains, but it differs in the binding of the remaining moieties: on the one hand, it lacks the P4 and P3' side chains;

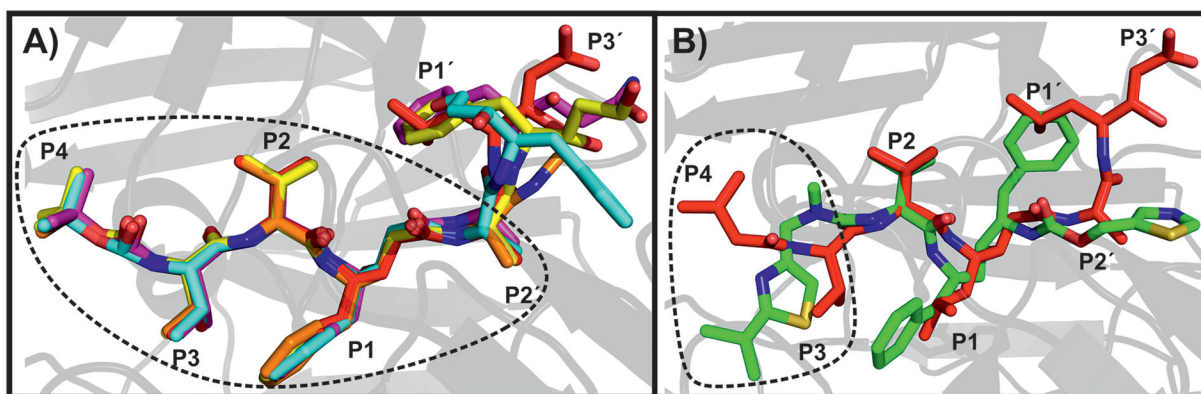


Figure 2. The binding mode of pepstatin A and the derived inhibitors (A) and ritonavir (B) in the active site of Sapp1p. The black dashed lasso highlights the molecular determinants important for inhibition (see the text). Colour coding: (A) pepstatin A – orange, KB32 – yellow, KB70 – magenta, KB74 – shorter, identical binding mode, thus hidden under the others, and KB75 – aquamarine. (B) ritonavir – green, pepstatin A – orange.

on the other hand, its P3 and P2' moieties extend further than those of pepstatin A (Figure 2(B)).

The interaction of the inhibitors in the Sapp1p-binding subsites

In all the crystal structures, we analysed hydrogen bonds and non-polar interactions. Pepstatin A and derived inhibitors form a total of 11–12 H-bonds with an average distance of 2.8–2.9 Å, whereas ritonavir make only eight H-bonds with an average distance of 3.0 Å. There are 11–12 nonpolar contacts for all the inhibitors except for the weakest pepstatin-based inhibitor KB74 (8) and ritonavir (9), with an average distance of 3.7–3.8 Å (Table 2). This smaller number of both hydrogen-bonding and nonpolar interactions probably contributes to the low affinity of ritonavir to Sapp1p.

Protein-ligand hydrogen-bonding interactions

As far as hydrogen-bonding interactions in the individual Sapp1p subsites are concerned, pepstatin A and four derived inhibitors exhibit strictly conserved hydrogen-bonding patterns in the S3–S1' subsites, including the catalytic aspartate dyad Asp32/Asp220, with heavy-atom distances differing at most by 0.3 Å (Table 1, Figure 3). This is contrasted to ritonavir, which lacks one hydrogen bond in the S3 pocket with Thr:OG1 due to the methylation of N74 in ritonavir and one in the S2 pocket with Asp80:OD2 due to its side-chain rotation (Figure 3). Furthermore, its hydrogen bond in the S1' pocket (Gly79) is substantially weakened because of slight adjustments of the backbones of both the protein and the ligand.

In the S2' pocket, pepstatin A and three pepstatin-based inhibitors (KB32, KB70 and KB74) form two hydrogen bonds to Sapp1p (Gly34:O and Asn125:ND2; Table 2(A)). KB75 lacks the latter one because of the different stereochemistry of the C-terminal Pst moiety and thus its inverted placement (Figure 2(A)). Ritonavir lacks the former one because of a slight repositioning of both the protein and ligand backbones.

The most variable region was the S3' pocket as a result of different P3' substituents – (3 R-4R)Pst for KB75, Pst for KB32 and KB70, missing moiety for KB74 and ritonavir, and Sta for pepstatin A. Only KB75 was able to form hydrogen bonds with Sapp1p (Arg77) thanks to its C-terminal Pst-moiety rotation (Table 2(A)).

Protein-ligand nonpolar interactions

The nonpolar contacts between Sapp1p and pepstatin-based inhibitors were mostly conserved with differences in distances up to 0.5 Å (Table 1(B)). In the S4 subsite, one nonpolar contact (Thr224) was missing for pepstatin A due to the different identity of the P4 substituent (isovaleric acid vs. tert-butyl-oxy-carbonyl in other pepstatin-based inhibitors). Both S4 nonpolar contacts (Thr224, Tyr285) were missing for ritonavir, which does not possess the P4 residues and forms different contacts in the S3 and S2 pockets (Pro112, Tyr227). In contrast to pepstatin-based inhibitors, ritonavir had different contacts in S3 and S2 pockets (Pro112, Tyr227). Larger changes were observed in the S1'/S3' pockets. Five contacts were present for pepstatin A, KB70, and KB32 (Ile303, Leu218, Asp301 and two from Gly79; Table 2(B)). KB75 lacked three of them but formed another two from Ala127 because of its different stereochemistry of the C-terminal Pst. KB74 does not possess the P3' substituent and thus did not have any S1'/S3' nonpolar contacts. Ritonavir formed only one nonpolar interaction in S1' (Ile303); one (Leu218) was missing as a result of the atom...atom distances slightly exceeding the threshold of 4.1 Å.

Discussion

The analysis of protein–inhibitor hydrogen-bonding and nonpolar contacts in crystal structures can be a useful tool for the interpretation of the molecular basis of differences in inhibitor affinities³⁹. In this work, we searched for structure–activity relationships (SAR) and found two molecular determinants of the inhibitor structures which defined their nanomolar affinity for Sapp1p. The first one was the conformation and orientation of the unprimed (P4–P1) and P2' side chains as well as the backbones of the KB70, KB75 and KB32 inhibitors in the Sapp1p binding cleft, which was nearly indistinguishable from the binding mode of pepstatin A (the black dashed lasso in Figure 2(A)). The presence of this trait is likely to have been, at least in part, responsible for the low nanomolar K_i values of these four inhibitors (from 0.1 to 6.6 nM; Figure 3). The absence of this characteristic feature (the missing P4 residue and the different orientation and contacts of the P3 residue of ritonavir; the black dashed lasso in Figure 2(B)) probably led to a significant affinity decrease (K_i : 1900 nM).

The second molecular determinant for the low nanomolar affinity of pepstatin A as well as three other Pst-containing inhibitors (KB70, KB75, and KB32) was the presence of the C-terminal extension beyond P2' (the cyan dashed lasso in Figure 3), forming nonpolar contacts in the S1' and S3' subsites (as they are adjacent

Table 2. (A) The hydrogen bonding of X-H...Y type, where X and Y are oxygen and nitrogen and (B) Nonpolar contacts of C...C type between Sappip and the four inhibitors studied here, pepstatin A and ritonavir. The atom...atom distances are in Å. The inhibitor names, composition and K_i values (nM) are indicated.

SUBSITE	PROTEIN (residue/name/atom)	LIGAND	Pepstatin		BocValValPstAlaPstNH ₂				Ritonavir		
			A	K _i = 0.3 nM	BocValValPstAlaPstNH ₂	BocValValPstAlaPstO	BocValValPstAlaPstO	BocValValPstAlaOMe		K _i = 1900 nM	
			KB 70		KB 75		KB 32		KB 74		
			K _i = 0.1 nM		K _i = 0.4 nM		K _i = 6.6 nM		K _i = 14.6 nM		
S3	Thr 224	Val2	N	3.0	2.9	2.9	2.9	2.9	2.9	n.d.*	n.d.*
	Thr 224	Val2	O	3.1	3.0	3.0	3.0	3.0	3.0	3.1	O76
S2	Asp 80	Val3	N	2.9	3.1	3.1	3.1	3.2	3.2	n.d.*	n.d.
	Asp 80	Val3	O	3.1	3.1	3.1	3.2	3.4	3.3	3.3	O61
S1	Gly 222	Sta/Pst	N	3.0	2.9	2.9	2.9	2.9	3.0	2.9	N58
	Asp 32	OD1	OH	2.5	2.5	2.5	2.5	2.5	2.5	2.4	O41
	Asp 220	OD1	OH	2.9	2.9	2.9	3.0	3.0	3.0	2.5	O41
	Asp 220	OD2	OH	2.4	2.4	2.4	2.4	2.5	2.5	2.9	O41
S1'	Gly 79	Sta/Pst	O	2.8	2.8	2.8	2.7	2.7	2.8	3.5	O24
S2'	Gly 34	Ala	N	2.8	2.8	2.8	2.9	2.9	2.9	n.d.	n.d.
S2'	Asn 125	Ala	O	3.0	3.1	3.1	3.3	3.3	3.1	3.3	N5
S3'	Arg 77	(3R-4R) Pst	N	n.d.	n.d.	2.8	n.d.	n.d.	n.d.	n.d.	n.d.
	Arg 77	(3R-4R) Pst	OH	n.d.	n.d.	3.6	n.d.	n.d.	n.d.	n.d.	n.d.
S4	Thr 224	CG2	Iva/Boc	n.d.*	CG2/C2	4.0	3.9	4.0	3.9	3.9	n.d.
	Tyr 285	CE1/CE2	Iva/Boc	3.5	CG2/C2	3.6	3.9	3.5	3.9	3.8	n.d.
S3	Pro 12	CG	Iva/Boc	n.d.	CG2/C2	n.d.	n.d.	n.d.	n.d.	n.d.	n.d.
S2	Ile 303	CD1	Val3	3.7	CG1	3.8	3.8	3.6	3.8	3.7	C64
	Tyr 227	CZ	Val3	n.d.*	CG1	n.d.*	n.d.*	n.d.*	n.d.*	n.d.*	C68
S1	Ile 30	CD1	Sta/Pst	3.8	CD1/CE1	3.6	3.3	3.5	3.3	3.6	C48/C49
	Tyr 78	CG/CB/CD1	Sta/Pst	3.5	CD2/CD2,CB	3.7	3.7	3.8	3.7	3.7, 3.9	C52, C14
	Val 113	CG1	Sta/Pst	n.d.	CZ	3.7	3.9	3.6	3.9	3.9	C49
	Ile 117	CD1	Sta/Pst	3.9, 3.9	CD1, CD2/CG/CD1, CD2	3.9	3.9	3.7	3.8	3.9	n.d.
S1'/S3'	Ile 303	CD1	Sta/Pst	3.9	CD1/CZ	3.6	3.5	n.d.	3.5	n.d.	C31
	Leu 218	CD2	Sta/Pst	3.8	CD2/CZ	3.8	4.0	n.d.	4.0	n.d.	n.d.
	Asp 301	CB	Sta/Pst	4.0	CD1/CE2	4.0	4.0	n.d.	4.0	n.d.	n.d.
	Ala 127	CA	Sta/Pst	n.d.	CZ	n.d.	n.d.	3.8	n.d.	n.d.	n.d.
	Ala 127	CB	Sta/Pst	n.d.	CE2	n.d.	n.d.	3.6	n.d.	n.d.	n.d.
	Gly 79	CA	Sta/Pst	4.1/3.7	CG/CD1/CE1/CM	3.9/4.0	4.0/4.0	3.8	4.0/4.0	n.d.	n.d.

*n.d. not determined.

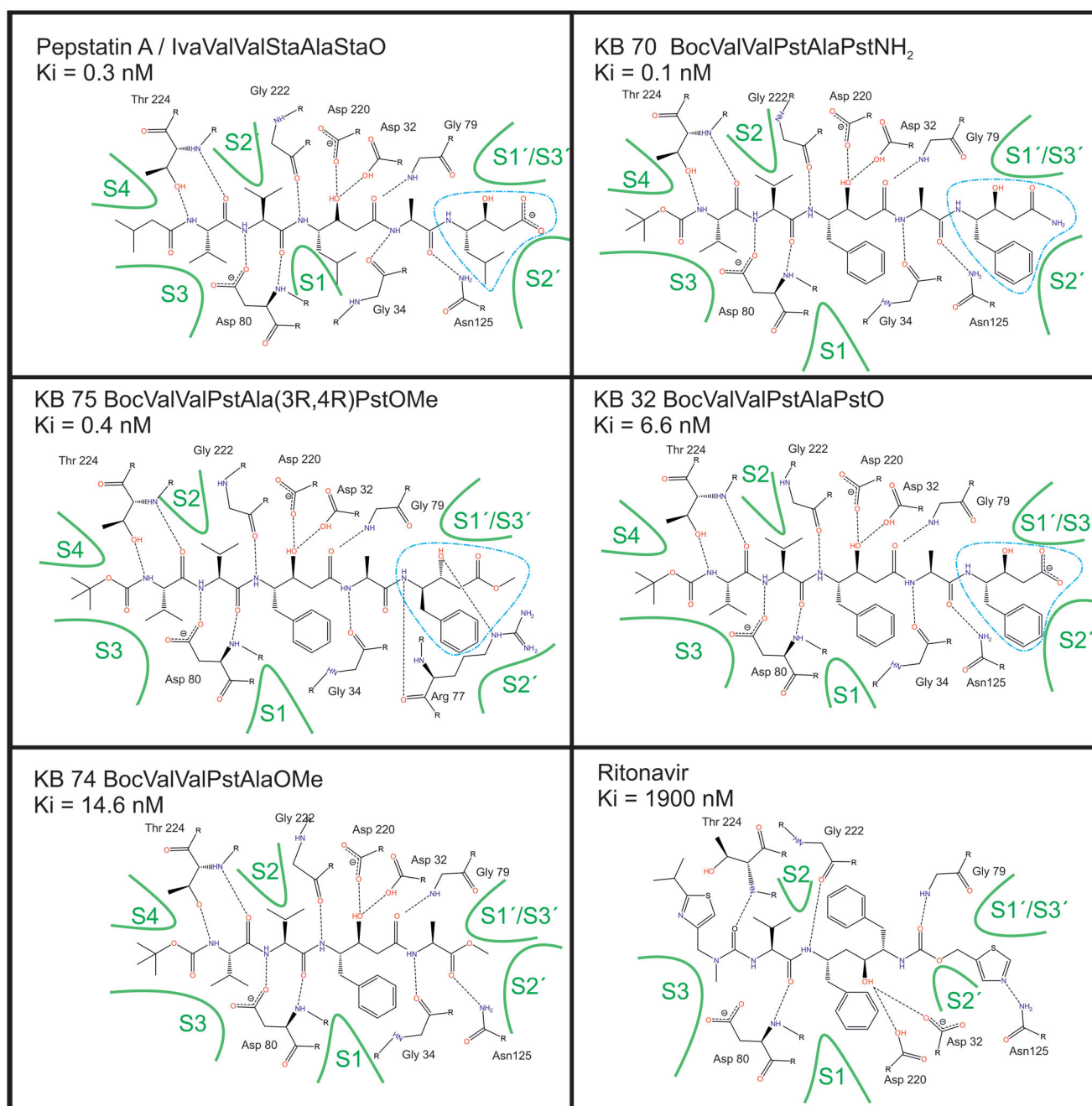


Figure 3. Schematic representations of hydrogen-bonding interactions and nonpolar contacts between Sapp1p and the six inhibitors studied here. The cyan dashed lasso shows the C-terminal extension beyond P2', which is the second determinant of nanomolar potency for the Pst-containing inhibitors (KB70, KB75 and KB32).

in the structure, they are collectively denoted as S1'/S3'). The absence of this extension in KB74 resulted in smaller numbers of hydrogen bonds as well as nonpolar contacts in the S1'/S3' sub-sites (cf. Table 2) and thus presumably in the lower affinity (K_i ; 14.6 nM).

Admittedly, it is beyond the capabilities of the used approach to pinpoint the fine structural determinants of potency between pepstatin A and the pepstatin-based inhibitors. One reason is the disorder in the crystal structures, which has prevented unequivocal localisation of the C-terminal parts of the pepstatin-based inhibitors as well as water molecules at the protein-inhibitor interface that may stabilise the complexes. Another factor is the dynamics of the inhibitor and the surrounding protein amino acids, which may also influence the binding affinities. Last but not least, quantum effects such as proton transfer may occur between

the active-site aspartates⁴⁰. Various computational approaches could be used to address these phenomena. Molecular dynamics (MD) can provide insights into the flexibility of the complexes and solvation patterns^{41,42}. MD-based energy analyses, such as the popular MM-GB/PBSA, are useful for obtaining interaction energies and their components and residue contributions^{43–45}. Quantum mechanics (QM) is a method of choice for cases where quantum effects play a role in protein–ligand binding^{31,46,47}.

Conclusions

We have determined four new crystal structures of nanomolar pepstatin-based inhibitors complexed to Sapp1p, an aspartic protease from the pathogenic yeast *Candida parapsilosis*. A

comparison of hydrogen bonding and nonpolar contacts with Sapp1p/pepstatin A and Sapp1p/ritonavir complexes has defined the molecular determinants responsible for high vs. low affinities. Most importantly, sub/low nanomolar inhibition occurred when the ligand filled the whole Sapp1p binding cavity from S4 to S3' pocket and formed numerous hydrogen bonds and nonpolar contacts. Such a structure-based insight can thus provide the basis for the development of novel medically useful compounds.

Disclosure statement

No potential conflict of interest was reported by the author(s).

Funding

ML, JD and IP were supported by the project 'Chemical Biology for Drugging Undruggable Targets' [ChemBioDrug CZ.02.1.01/0.0/0.0/16_019/0000729] from the European Regional Development Fund (OP RDE). JD, JB, IP, OH and ML were supported by the institutional project RVO 61388963 and LV by the project RVO 86652036. ML was supported by the Ministry of Education, Youth and Sports of the Czech Republic from the Large Infrastructures for Research, Experimental Development, and Innovations project 'IT4 Innovations National Supercomputing Center – LM2015070'.

ORCID

Iva Pichová  <http://orcid.org/0000-0002-2178-9819>

Martin Lepšík  <http://orcid.org/0000-0003-2607-8132>

References

- Toth R, Nosek J, Mora-Montes HM, et al. *Candida parapsilosis*: from genes to the bedside. *Clin Microbiol Rev* 2019;32:e00111-18.
- Prasad R, Shah AH, Rawal MK. Antifungals: mechanism of action and drug resistance. *Adv Exp Med Biol* 2016; 892: 327–49.
- Baddley JW, Patel M, Bhavnani SM, et al. Association of fluconazole pharmacodynamics with mortality in patients with candidemia. *Antimicrob Agents Chemother* 2008;52:3022–8.
- Lohse MB, Gulati M, Craik CS, et al. Combination of antifungal drugs and protease inhibitors prevent *Candida albicans* biofilm formation and disrupt mature biofilms. *Front Microbiol* 2020;11:1027.
- Hruskova-Heidingsfeldova O. Secreted proteins of *Candida albicans*. *Front Biosci* 2008;13:7227–42.
- Winter MB, Salcedo EC, Lohse MB, et al. Global identification of biofilm-specific proteolysis in *Candida albicans*. *mBio* 2016;7:
- Naglik JR, Rodgers CA, Shirlaw PJ, et al. Differential expression of *Candida albicans* secreted aspartyl proteinase and phospholipase B genes in humans correlates with active oral and vaginal infections. *J Infect Dis* 2003;188:469–79.
- Cassone A, De Bernardis F, Torosantucci A, et al. *In vitro* and *in vivo* anticandidal activity of human immunodeficiency virus protease inhibitors. *J Infect Dis* 1999;180:448–53.
- Bektic J, Lell CP, Fuchs A, et al. Hiv protease inhibitors attenuate adherence of *Candida albicans* to epithelial cells *in vitro*. *FEMS Immunol Med Microbiol* 2001;31:65–71.
- Schaller M, Bein M, Korting HC, et al. The secreted aspartyl proteinases sap1 and sap2 cause tissue damage in an *in vitro* model of vaginal candidiasis based on reconstituted human vaginal epithelium. *Infect Immun* 2003;71:3227–34.
- Borg-von Zepelin M, Meyer I, Thomssen R, et al. Hiv-protease inhibitors reduce cell adherence of *Candida albicans* strains by inhibition of yeast secreted aspartic proteases. *J Invest Dermatol* 1999;113:747–51.
- Fallon K, Bausch K, Noonan J, et al. Role of aspartic proteases in disseminated *Candida albicans* infection in mice. *Infect Immun* 1997;65:551–6.
- Korting HC, Schaller M, Eder G, et al. Effects of the human immunodeficiency virus (hiv) proteinase inhibitors saquinavir and indinavir on *in vitro* activities of secreted aspartyl proteinases of *Candida albicans* isolates from hiv-infected patients. *Antimicrob Agents Chemother* 1999;43:2038–42.
- Cenci E, Francisci D, Belfiori B, et al. Tipranavir exhibits different effects on opportunistic pathogenic fungi. *J Infect* 2008;56:58–64.
- Braga-Silva LA, Mogami SS, Valle RS, et al. Multiple effects of amprenavir against *Candida albicans*. *FEMS Yeast Res* 2010; 10:221–4.
- Li C, Liu Y, Wu S, et al. Targeting fungal virulence factor by small molecules: structure-based discovery of novel secreted aspartic protease 2 (sap2) inhibitors. *Eur J Med Chem* 2020; 201:(112515
- Dong G, Liu Y, Wu Y, et al. Novel non-peptidic small molecule inhibitors of secreted aspartic protease 2 (sap2) for the treatment of resistant fungal infections. *Chem Commun* 2018;54:13535–8.
- Horvath P, Nosanchuk JD, Hamari Z, et al. The identification of gene duplication and the role of secreted aspartyl proteinase 1 in *Candida parapsilosis* virulence. *J Infect Dis* 2012; 205:923–33.
- Singh DK, Nemeth T, Papp A, et al. Functional characterization of secreted aspartyl proteases in *Candida parapsilosis*. *mSphere* 2019;4:e00484-19.
- Wlodawer A, Vondrasek J. Inhibitors of hiv-1 protease: a major success of structure-assisted drug design. *Annu Rev Biophys Biomol Struct* 1998; 27:249–84.
- Dunn BM. Structure and mechanism of the pepsin-like family of aspartic peptidases. *Chem Rev* 2002;102:4431–58.
- Hruskova-Heidingsfeldova O, Dostal J, Majer F, et al. Two aspartic proteinases secreted by the pathogenic yeast *Candida parapsilosis* differ in expression pattern and catalytic properties. *Biol Chem* 2009;390:259–68.
- Dostal J, Brynda J, Hruskova-Heidingsfeldova O, et al. The crystal structure of the secreted aspartic protease 1 from *Candida parapsilosis* in complex with pepstatin A. *J Struct Biol* 2009;167:145–52.
- Umezawa H, Aoyagi T, Morishima H, et al. Pepstatin, a new pepsin inhibitor produced by actinomycetes. *J Antibiot* 1970;23:259–62.
- Pichova I, Pavlickova L, Dostal J, et al. Secreted aspartic proteases of *Candida albicans*, *Candida tropicalis*, *Candida parapsilosis* and *Candida lusitanae*. Inhibition with peptidomimetic inhibitors. *Eur J Biochem* 2001;268:2669–77.
- Houstecka R, Hadzima M, Fanfrik J, et al. Biomimetic macrocyclic inhibitors of human Cathepsin D: structure-activity relationship and binding mode analysis. *J Med Chem* 2020; 63:1576–96.
- Cadicamo CD, Mortier J, Wolber G, et al. Design, synthesis, inhibition studies, and molecular modeling of pepstatin

- analogues addressing different secreted aspartic proteinases of *Candida albicans*. *Biochem Pharmacol* 2013;85:881–7.
28. Gruber A, Berlit J, Speth C, et al. Dissimilar attenuation of candida albicans virulence properties by human immunodeficiency virus type 1 protease inhibitors. *Immunobiology* 1999;201:133–44.
 29. Gruber A, Speth C, Lukasser-Vogl E, et al. Human immunodeficiency virus type 1 protease inhibitor attenuates *Candida albicans* virulence properties *in vitro*. *Immunopharmacology* 1999;41:227–34.
 30. Skrbec D, Romeo D. Inhibition of candida albicans secreted aspartic protease by a novel series of peptidomimetics, also active on the hiv-1 protease. *Biochem Biophys Res Commun* 2002;297:1350–3.
 31. Dostal J, Pecina A, Hruskova-Heidingsfeldova O, et al. Atomic resolution crystal structure of sapp2p, a secreted aspartic protease from *Candida parapsilosis*. *Acta Crystallogr D Biol Crystallogr* 2015;71:2494–504.
 32. Dostal J, Brynda J, Hruskova-Heidingsfeldova O, et al. The crystal structure of protease sapp1p from candida parapsilosis in complex with the hiv protease inhibitor ritonavir. *J Enzyme Inhib Med Chem* 2012;27:160–5.
 33. Merkerova M, Dostal J, Hradilek M, et al. Cloning and characterization of sapp2p, the second aspartic proteinase isoenzyme from *Candida parapsilosis*. *FEMS Yeast Res* 2006;6:1018–26.
 34. Mueller U, Förster R, Hellmig M, et al. The macromolecular crystallography beamlines at bessy ii of the helmholtz-zentrum berlin: current status and perspectives. *Euro Phys J Plus* 2015;130:141.
 35. Winn MD, Ballard CC, Cowtan KD, et al. Overview of the ccp4 suite and current developments. *Acta Crystallogr D Biol Crystallogr* 2011;67:235–42.
 36. Murshudov GN, Skubak P, Lebedev AA, et al. Refmac5 for the refinement of macromolecular crystal structures. *Acta Crystallogr D Biol Crystallogr* 2011;67:355–67.
 37. Salentin S, Schreiber S, Haupt VJ, et al. Plip: fully automated protein-ligand interaction profiler. *Nucleic Acids Res* 2015;43:W443–447.
 38. Pettersen EF, Goddard TD, Huang CC, et al. Ucsf Chimera-a visualization system for exploratory research and analysis. *J Comput Chem* 2004;25:1605–12.
 39. Kozisek M, Lepsik M, Grantz Saskova K, et al. Thermodynamic and structural analysis of hiv protease resistance to darunavir – analysis of heavily mutated patient-derived hiv-1 proteases. *Febs J* 2014;281:1834–47.
 40. Northrop DB. Follow the protons: a low-barrier hydrogen bond unifies the mechanisms of the aspartic proteases. *Acc Chem Res* 2001;34:790–7.
 41. De Vivo M, Masetti M, Bottegoni G, Cavalli A. Role of molecular dynamics and related methods in drug discovery. *J Med Chem* 2016;59:4035–61.
 42. Spitaleri A, Zia SR, Di Micco P, et al. Tuning local hydration enables a deeper understanding of protein-ligand binding: the pp1-src kinase case. *J Phys Chem Lett* 2021; 12: 49–58.
 43. Gemperle J, Hexnerova R, Lepsik M, et al. Structural characterization of cas sh3 domain selectivity and regulation reveals new cas interaction partners. *Sci Rep* 2017;7:8057
 44. Wang W, Kollman PA. Computational study of protein specificity: the molecular basis of hiv-1 protease drug resistance. *Proc Natl Acad Sci USA* 2001;98:14937–42.
 45. Lepsik M, Kriz Z, Havlas Z. Efficiency of a second-generation hiv-1 protease inhibitor studied by molecular dynamics and absolute binding free energy calculations. *Proteins* 2004;57: 279–93.
 46. Pecina A, Eyrilmez SM, Köprülüoğlu C, et al. Sqm/cosmo scoring function: reliable quantum-mechanical tool for sampling and ranking in structure-based drug design. *Chempluschem* 2020;85:2362–71.
 47. Cavasotto CN, Adler NS, Aucar MG. Quantum chemical approaches in structure-based virtual screening and lead optimization. *Front Chem* 2018;6:188.